SAND98-1735C
SAND--98-1735C

CREEP FAILURE OF A REACTOR PRESSURE VESSEL LOWER HEAD UNDER SEVERE ACCIDENT CONDITIONS

CONF-980708--

M. M. Pilch[a], Y. R. Rashid[b], J. S. Ludwigsen,[a], and T. Y. Chu[a]

[a]Sandia National Laboratories
P.O. Box 5800-1139
Albuquerque N.M. 87185
ph (505) 845 3047
email mpilch@sandia.gov

[b]ANATECH
5435 Oberlin Dr.
San Diego, CA 92121
ph (619) 455 6350

ABSTRACT

A severe accident in a nuclear power plant could result in the relocation of large quantities of molten core material onto the lower head of the reactor pressure vessel (RPV). In the absence of inherent cooling mechanisms, failure of the RPV ultimately becomes possible under the combined effects of system pressure and the thermal heat-up of the lower head. Sandia National Laboratories has performed seven experiments at 1:5th scale simulating creep failure of a RPV lower head. This paper describes a modeling program that complements the experimental program.

Analyses have been performed using the general-purpose finite-element code ABAQUS-5.6. In order to make ABAQUS solve the specific problem at hand, a material constitutive model that utilizes temperature dependent properties has been developed and attached to ABAQUS-executable through its UMAT utility. Analyses of the LHF-1 experiment predict instability-type failure. Predicted strains are delayed relative to the observed strain histories. Parametric variations on either the yield stress, creep rate, or both (within the range of material property data) can bring predictions into agreement with experiment. The analysis indicates that it is necessary to conduct material property tests on the actual material used in the experimental program. The constitutive model employed in the present analyses is the subject of a separate publication.

INTRODUCTION

In the event of a core melt accident, the lower head of the reactor pressure vessel can be subjected to significant thermal and pressure loads, which if they persist, can eventually lead to the failure of the lower head by creep rupture. The mode, timing, and size of lower head failure are of prime importance in the assessment of core melt accidents because they define the initial conditions for ex-vessel events such as core/basemat interactions, fuel/coolant interactions, and direct containment heating. On the other hand, recent studies indicate that the deformation of a reactor vessel lower head due to creep may be a precursor to water ingression between the melt mass and the vessel wall, leading to the possibility of in-vessel core retention without external cooling. Therefore, from both an accident assessment and accident mitigation considerations, there is a need to understand the mechanism of lower head creep deformations and failure, and based on this understanding to develop a predictive capability.

International efforts to model the TMI-II accident have generally predicted creep failure of the vessel where, as it is well known, no failure or observable creep deformations occurred. Therefore, there has been a need for large-scale integral tests to validate model predictions as the technical community continues to improve and further develop their modeling capabilities. The LHF program at Sandia National Laboratories was developed for this purpose.

Sandia has performed seven large-scale experiments simulating creep failure of the RPV lower head under different thermal and pressure loading conditions. Scaling analyses (Chu et al. 1997) showed that geometrically scaled experiments can be conducted at reduced scale if the heat flux to the lower head is scaled by the facility scale factor.

DISCLAIMER

In addition, the scaling analysis concludes that prototypic materials must be used for the RPV mockup. Implications of the scaling analyses are that the heat-up and creep time scales are preserved while decreasing the temperature drop across the vessel.

LHF-1 EXPERIMENT

A schematic and an overall view of the experiment are shown respectively in Figures 1 and 2. The Apparatus is basically a scaled version of the lower part of a TMI-like reactor pressure vessel (RPV) without the vessel skirt, consisting of a hemispherical head made of SA533B1 steel, and a 30 cm cylindrical section replicating the lower part of the RPV cylindrical wall. The inner-diameter of the lower head is 0.91 m, and the wall thickness is typically 30 mm, corresponding to a geometrical scale factor of 4.85. Due to the forming operation, a small region of the wall at the bottom is slightly thinner (~28mm).

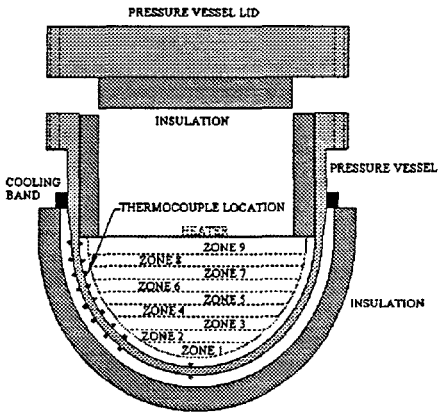

Schematic of LHF Test Apparatus

Figure 1: Schematic of LHF test apparatus

The energy transfer to the reactor vessel from the core debris is simulated using a hemispherical resistive heater (Fig. 1). The heater is built in three sections, each with three independently controlled heater segments, for a total of nine segments. For experiments with localized peaks "fences" made of insulation felt are used to isolate (the radiation of) the three heater sections to better achieve localized heating of the vessel bottom. The inner surface of the bottom head is painted with a Pyromark^{R} black for efficient radiation absorption. The outer surface of the bottom head and the inner surfaces of the cylindrical section and the top flange are insulated. A cooling band is provided at the transition between the spherical and the cylindrical sections to simulate the proper far field temperature condition (due the presence of water in the RPV).

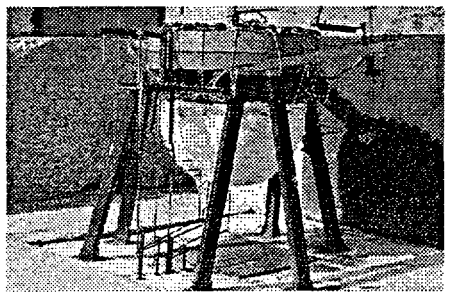

Figure 2: LHF test vessel and support

Thermocouples are used to measure wall temperature and through-the-wall temperature difference. Locations on the hemisphere are described in terms of "longitude" and "latitude." The equator of the bottom head is defined as having 0° latitude and the pole is defined as having 90° latitude. There are two major arrays (A and B) of arranged thermocouples, 90° apart, to measure the interior wall temperature from the equator to the bottom of the vessel. There is also a matching array of exterior thermocouples for array B. The latitudinal locations of the thermocouples correspond to the center of each heater segment. Figure 3 shows the temperature history in the LHF-1 experiment. The vessel was heated uniformly from the bottom (90°) to 30°. Temperatures tapered off from 30° up to the equator (0°). The temperature difference across the vessel wall is ~5 °C.

The pressure load is provided by a manifold of bottled argon and by heating of the confined gas within the test vessel itself. Pressure of the vessel is controlled by automatic fill and bleed valves once the operating pressure for the experiment is achieved. For the LHF-1 experiment, the operating pressure for the test was reached at ~90 min and held constant at 10 MPa until failure of the vessel.

Linear displacement transducers are used to monitor the deformation of the test vessel. Displacement transducers are deployed along a chosen longitude at 30°, 60°, and 90° latitude. At 30° and 60°, there are two transducers to measure

both the vertical and horizontal displacements. Figure 3 shows the displacements during the test. The shape and the local wall thickness of the vessel are measured before and after the experiment for comparison. A grid system, made visible with punch marks on the vessel surface, is used to map local deformation as well as change in wall thickness. The grid system has a 5^0 by 5^0 pitch over the entire hemispherical head. Figure 4 shows the post-test view of the failed vessel.

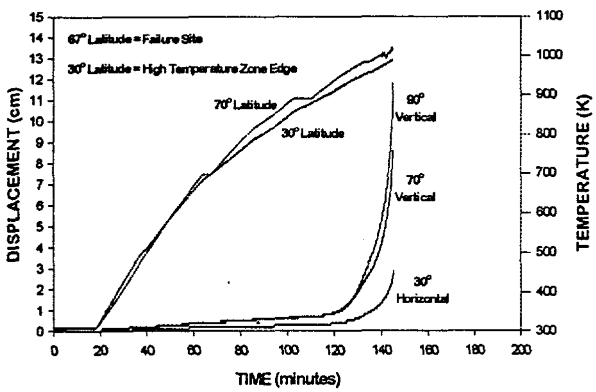

Figure 3: LHF-1 test conditions and results

Figure 4: Post-test view of the failed LHF-1 test vessel

MATERIAL PROPERTY CURVEFITS

Elastic/plastic and creep properties for SA533B1 steel are highly temperature dependent. Existing data (300K<T<1250K) have been gathered from the literature (Diercks, 1994; Rempe, 1993; NRIM, 1987; Reddy, 1982; and McCoy, 1989) for the elastic modulus (E), yield strength (σ_y), true ultimate stress (σ_u), and the plastic modulus (E_p). These temperature dependent material properties can all be fit to an empirical function of he form

$$\varphi = \frac{A}{\epsilon + \left(\frac{T}{B}\right)^{C}} e^{N(\epsilon,\sigma_{err})} \tag{1}$$

where φ is the specific material property, T is the temperature in degrees Kelvin, and A, B, and C fitting parameters. There is an abundance of data from room temperature up to ~250°C above normal operating conditions (300K<T<850K), and only limited data for severe accident conditions (850K<T<1250K). Consequently, the curvefits were performed by weighing the high temperature data more heavily so that the low temperature data did not dominate the fitting process in the high temperature regimes of interest to severe accident analyses. Table 1 summarizes the fitting constants for each property. The goodness of fit is characterized by the regression coefficient, r^2. Figures 5 and 6 show that the properties decrease significantly with temperature.

1					
				1	1_{err}
(G)	22 6	84 3	4 8553	0 859	0 2 0
1_y(M)	463 84	865 6	9 6227	0 950	0 4
1_u(M)	225 0	933 35	2 999	0 748	0 28
$_p$(G)	3 2023	877 7	9 4646	0 882	0 62

Uncertainties in the material properties are represented by the normal standard variable N(0, σ_{err}) where

1 1
1 Ⅱ Ⅱ 1
1 1 (2)
1 1
1
1

is the standard deviation of the natural logs of curvefit predictions ($\phi_{p,i}$) and data measurements ($\phi_{m,i}$). The natural log is required because the dependent variables vary over several orders of magnitude on the temperature range of interest and

the errors are normally distributed in this format. The material property uncertainties are large (e.g., the uncertainty on the yield stress is +/- 30% for two standard deviations. Careful examination of the database shows that variations are much smaller for any given "batch" of sample material. The large variations are realized when measurements from one batch are compared to measurements from another batch, even when each batch is nominally the same material with the same heat treatment. Variations also potentially arise from seemingly insignificant variations of material composition (within ASME specifications) or seemingly insignificant variations in heat treatment.

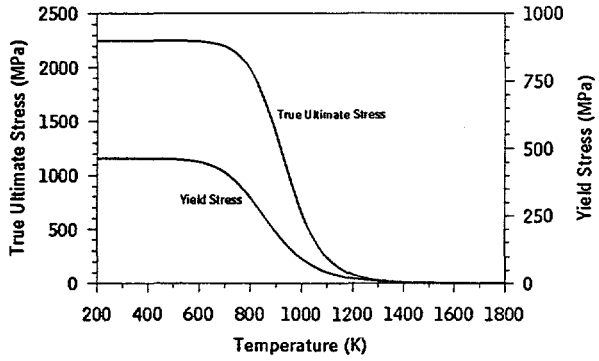

Figure 5: Yield stress and true ultimate stress for SA533B1 steel

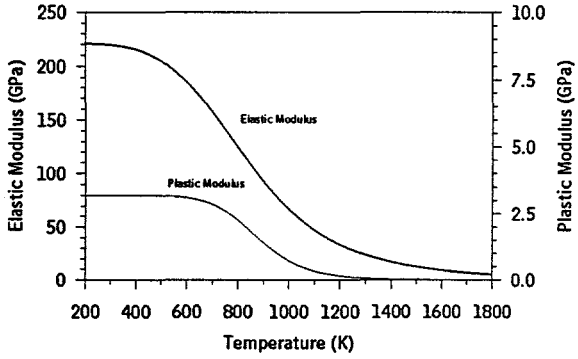

Figure 6: Elastic modulus and plastic modulus for SA533B1 steel

Large temperature changes during vessel heat-up give rise to thermal expansion. The thermal expansion coefficient is empirically fit to data in Reddy and Ayres (1982),

$$\alpha = -5.352 + 0.7320T^{0.5} + \frac{63.28}{T} \quad (\mu m/m/^{\circ}C), \quad (3)$$

The goodness of fit is near perfect for the single-source and limited data on which this function is based.

Creep data for SA533B1 steel is available in the form of engineering strain versus time (Rempe, 1993, and Diercks, 1994). Each test is conducted under constant load (not constant stress) and constant temperature conditions. The traditional approach is to fit a power law function of the form

$$\varepsilon = A\sigma_o^m t^n \quad (4)$$

to the experimental data where σ_0 is the stress at the start of the creep test before any elongation and necking occurs. Under severe accident conditions (T>850K), the quantity "A" is a hypersensitive function of temperature, varying ~6 or 7 orders of magnitude for temperatures ranging from 850K to 1373K.

We have found that the temperature sensitivity of all fitting parameters can be correlated with the following functional form for the parameter A in Eq. 4.

$$A = \left(\frac{1}{\sigma_y(T)}\right)^m e^{-T_{ref}/T} \frac{1}{t_{ref}^n} e^{N(0,\sigma_{err})} \quad (5)$$

This empirical formulation was motivated by a desire to normalize the stress such that it is bounded by order unity. The constants m, T_{ref}, n, and t_{ref} are fitting parameters that depend on temperature in a step-wise fashion as shown in Table 2. Creep tests show that primary creep is typically negligible, secondary creep is a linear function of time (n=1), and tertiary creep is a power law (n>1) in time. Although the exponential term involves temperature, normalizing the stress with the temperature dependent yield stress dominates the temperature effects. The fitting procedure involves finding values for A and n for a given test (i.e., σ_0 and T fixed). Looking at the ensemble of n and A values from the complete database, we find that the parameter n is independent of temperature and stress and that the A values can be fit to the function above to establish the fitting parameters m, T_{ref}, and t_{ref}. Uncertainties in the correlation for A are reflected in

the normal distribution of logarithmic errors as reflected in $N(0,\sigma_{err})$.

Table 2 summarizes the fitting parameters for secondary and tertiary creep. The tertiary creep parameters are included here for completeness even though they are not used in the current analyses for reasons discussed latter. SA533B1 steel exhibits a phase transition between 1000K and 1100K, so it is necessary to have separate fits above and below the mid-transition temperature of 1050K. The creep database used here for severe accident analyses spans the temperature range of 873K to 1373K. The database was restricted to include only those tests where the initial stress was less than the yield stress at the test temperature. The goodness of fit is characterized by the regression coefficient, r^2. $N(0,\sigma_{err})$ is a normal standard variable with mean zero and a relative standard deviation based upon the natural log of predictions and measurements, similar to Eq. 2.

Table 2. Creep Law Fitting Parameter		
Secondary Creep	850K<T	1050K<T
m	4.5480	4.1706
T_{ref}(K)	17084	3193
n	1.0	1.0
t_{ref}(hr)	8.7258×10^{-8}	1.0002
r^2	0.892	0.790
σ_{err}	0.493	0.627
Tertiary Creep		
m	10.851	7.9287
T_{ref}(K)	45078	5378
n	2.386	2.386
t_{ref}(hr)	2.9296×10^{-4}	1.0000
r^2	0.797	0.709

IMPLEMENTATION OF THE CONSTITUTIVE MODEL

As is generally the case, material property tests are rarely conducted simultaneously with, or for the purpose of, the development of constitutive models; the latter usually follows long after the data were obtained. Since the primary purpose of constitutive models is to be used to predict the behavior of structures and physical model experiments for which material properties tests are needed, it follows that the two activities should be joined. In the present case, however, the material properties data was obtained from various archival sources and, therefore, is two steps removed from the constitutive model development for use in the LHF-1 experiment: Firstly, the LHF-1 specimen is manufactured by a material forming process that is different from the test specimens. Secondly, the material properties data, which came from various laboratories, has not been subjected to the rigorous consistency check usually provided by constitutive behavioral modeling. Thus, the task at hand is to adapt the available data to an existing constitutive model, making necessary simplifying assumptions.

As mentioned in the preceding section, the data was separated into two groups: Time-independent properties and creep data. With regards to the time-independent properties, the developed relations are based on the assumption that in a high temperature test where transient creep can be difficult to separate from the elastic/plastic response, the material's instantaneous response can not be accurately measured. Similarly, in developing creep relations, the assumption that is usually made is that data from constant-load creep tests can be used directly in a creep law which, by definition, implies that the stress (and temperature) are constant with time. In a constant-load creep test the stress rises due to the reduction in area with time, eventually leading to the so-called tertiary creep. In a properly posed large-deformation analysis the change in the stress due to the change in geometry is already accounted for in the constitutive model and, therefore, it is incorrect to treat tertiary creep as a material property. Ignoring the tertiary creep data greatly simplifies the task of defining the parameters in the creep formula by restricting the data-fitting process to the minimum creep rate in the low strain range where the stress can be considered to be constant. In this manner, the measured creep rate expression can be used directly in the constitutive model where the true stress is the quantity used. Other constitutive properties such as the true stress-true strain curve are transformed within the constitutive routine to engineering stress-engineering strain to enable the use of measured data.

With the simplifying assumptions stated above, it is possible to adapt an existing large-strain viscoplastic constitutive software (Rashid, 1997) to

the data described in the preceding section. This constitutive model integrates the constitutive equations for von Mises viscoplasticity with isotropic hardening, using the material's elasto-plastic properties and a uniaxial stress-strain and strain-rate equation in the inelastic regime of the following form.

$$\sigma = K\varepsilon^{\alpha}\left(\frac{\dot{\varepsilon}}{\dot{\varepsilon}_0}\right)^{\beta} \qquad (6)$$

where σ=stress, ε=strain; $\dot{\varepsilon}$=strain rate, $\dot{\varepsilon}_0$=reference strain rate, K=strength coefficient, α=hardness coefficient, β=strain-rate sensitivity coefficient.

The constants K, α, and β can be determined by solving Eq. 6 and equating the result to the time derivative of Eq. 4, which results in the following relations:

$$\dot{\varepsilon} = \dot{\varepsilon}_0\left(\frac{\sigma}{K}\right)^{1/\beta}\varepsilon^{\alpha/\beta} \qquad (7)$$

where

$$\alpha = (1-n)/m$$
$$\beta = n/m$$
$$K = \left(n^{n}A\right)^{-1/m}$$
$$\dot{\varepsilon} = 1$$

Care must be taken to convert the true stresses calculated by the code into an effective engineering stress before evaluating the creep correlation, which is fit to a database where only engineering strains are reported.

The input to the constitutive model consists of the stress and strain information from the previous step together with the stretching rates computed in the step and the increment of time. It returns the updated Cauchy (true) stresses, the stress-strain tangent modulus matrix and the updated state variables. The model first computes the directions and magnitudes of the Cauchy stresses using an iteration procedure and assuming that the stretching rates are constant over the step. Once the stresses are updated, the tangent moduli are computed by applying a perturbation method to the constitutive equations. Specifically, the 6x6 tangent modulus matrix with 21 independent components is the square matrix that relates the slight variations in input strain increments $d\varepsilon_{ij}$ to the corresponding variations in updated stresses $d\tau_{ij}$. A more complete description of the constitutive model is reserved for a later publication.

ANALYSIS RESULTS

The constitutive model with the material properties data base described in the preceding sections were utilized in the analysis of the LHF-1 experiment using the ABAQUS finite element program. The creep relations used in the constitutive model consist only of the secondary creep rate derived from Eq. 5 with n=1, excluding the primary creep because of its small magnitude and disregarding tertiary creep for the reasons mentioned earlier. In order to demonstrate that tertiary creep is not a material property but merely the material's creep response to a continuously increasing stress resulting from deformation and necking, an analysis of one of the creep tests (T=973K, σ_0=80 MPa) from the data base was carried out using the constitutive model with only secondary creep. Figure 7 shows the predicted results compared to measured data. As can be seen the analysis results exhibit the observed tertiary creep behavior although the constitutive model is based on secondary creep only.

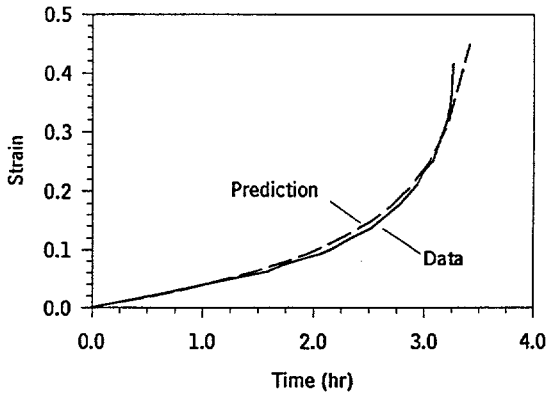

Figure 7: Prediction of a constant load creep test

The analysis of the LHF-1 experiment utilized a grid with 5 x 90 8-node axisymmetric solid elements (5 through the thickness with 1° subtended angle). The local variation in thickness in the bottom region

was incorporated in the finite element mesh. The thermal and pressure input were the experimentally measured temperature and pressure histories. Several analyses were conducted, the first of which is based on the default constitutive model described in the preceding section. The other analyses use variations on material parameters as described below.

Figure 8 compares the observed vertical displacements at the bottom of the vessel with predictions for the default constitutive model. Thermal expansion dominates observed displacements for times less than ~120 min in the experiment. After ~120 min, the vertical displacements increase very rapidly until failure at ~145 min. The observed vessel temperature is ~950K at the onset of large deformations. The model prediction captures the basic trends; however, the thermal expansion is somewhat under-predicted and the onset of very large deformations leading to instability-type failure is delayed by about 10 minutes relative to the experimental observations. In addition, the predictions exhibit a steeper slope after the onset of large deformations.

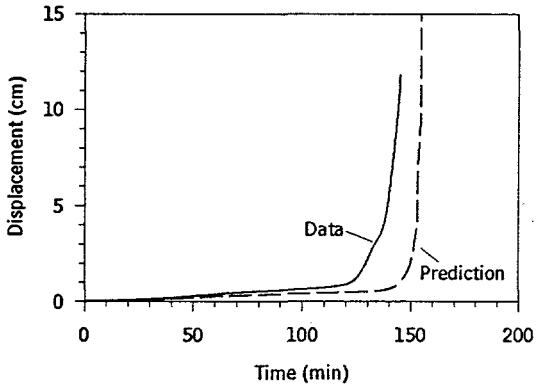

Figure 8: Predicted and measured vertical displacement using the default constitutive model

We note that there are significant uncertainties in the material property database. Large deformations can initiate at 120 min and lead to failure at ~145 min if the steel used in the test yields at a lower temperature or if the creep rates are higher in the test steel, both relative to the material property correlations. We explored the possibility that the key material properties in the test fixture may deviate in a systematic fashion from the material property corrrelations by placing independent multipliers on the material parameter $\sigma_y(T)$, which appears in Eq.5 and on the creep rate in Eq. 7. These two multipliers were varied seperately and in combination until the predicted failure time coincides with the observed failure time. These three sensitivity cases are compared to the experimental data in Figure 9.

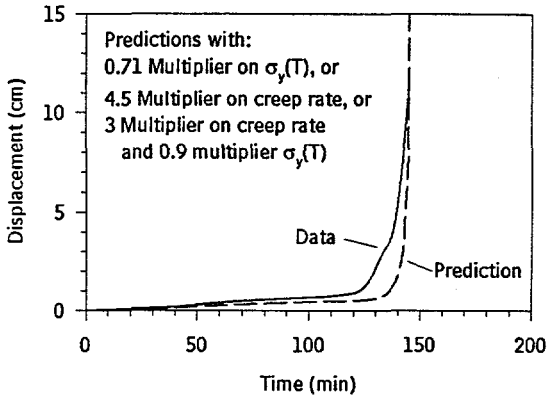

Figure 9: Predicted and measured vertical displacements for various multipliers and constitutive model parameters

The multipliers so derived are plausible in the sense that the material property variations within the scatter of the available database can reproduce the experiment observations. As expected, all three variations gave almost identical results since the creep rate and the material parameter A are inter-related through Eqs. 4 and 5. We expect that an optimal prediction of the experimental data can be obtained through a reformulation of the fitted parameters rather than by simple multipliers. This will have to be aided by an experimental program as discussed below.

We recommend a two step approach towards resolving whether deviations between base predictions and observations are a result of model deficiencies or whether they are a result of material property uncertainties. First, we will perform limited material property tests on the steel actually used in the LHF tests in order to spot check whether the material used in the LHF program is consistent with the existing material property database as reflected in our correlations. Secondly, we will make predictions for the other tests in the LHF test series (with different thermal and pressure histories) using a consistent set of multipliers. These activities are sufficient to assess whether the model proposed here is adequate for reactor applications.

ACKNOWLEDGMENTS

This work was supported by the U.S. Nuclear Regulatory Commission and was performed at Sandia National Laboratories, which is operated for the U.S. Department of Energy under Contract No. DE-AC04-94AL85000.

References

Chu, T.Y., M.M. Pilch, and J.H. Bentz (Nov. 16-20, 1997) "An Assessment of the Effects of Heat Flux Distribution and Penetration on the Creep Rupture of a Reactor Pressure Vessel," Twelfth Proceedings of Nuclear Thermal Hydraulics, 1997 ANS Winter Meeting, Albuquerque, NM.

Diercks, D.R., and L.A. Neimark (1994) "Results of Mechanical Tests and Supplementary Microstructural Examinations of the TMI-2 Lower Head Samples," NUREG/CR-6189.

McCoy (1989), "Tensile and Creep Properties of SA533 Grade B Class 1 Steel," DOE-HTGR-88383.

NRIM (1987), "NRIM Creep Data Sheet No. 18B," National Research Institute For Metals, Tokyo, Japan.

Rashid, Y.R., "Creep Considerations for the Lower Head," Nuclear Engineering and Design 169 (1997), 101-108.

Reddy, G.B., and D.J. Ayres (1982), "High Temperature Elastic-Plastic and Creep Properties for SA533 Grade B Class 1 and SA508 Materials," EPRI-NP-2753.

Rempe et al. (1993), "Light Water Reactor Lower Head Failure Analysis," NUREG/CR-5642.